CLOUD TOP TEMPERATURE IN A LARGE RAINSTORM

An Interim Report to
National Ocean and Atmospheric Administration

A REPORT

from the space science and engineering center
the university of wisconsin-madison
madison, wisconsin

CLOUD TOP TEMPERATURE IN A LARGE RAINSTORM

An Interim Report to
National Ocean and Atmospheric Administration

Contract # NA-84-DCG-00240

University Account # 144-W107

for the period of

28 September 1984 through 27 September 1985

Submitted by

David W. Martin

Space Science and Engineering Center
at the University of Wisconsin-Madison
1225 West Dayton Street
Madison, Wisconsin 53706
(608) 262-0544

December 1985

ABSTRACT

For a single complex of cumulonimbus clouds rainrate has been related to cloud top temperature and to the structure (variability) of cloud top temperature. Rainrate was inferred from ppi scans of the Monett, MO, National Weather Service radar. Cloud top temperature was inferred from thermal infrared images of a Geostationary Operational Environmental Satellite.

An analysis of radar and satellite image pairs indicated a useful correspondence of echoes and cloud top structure on scales of 50 km and larger. On scales larger than 50 km but still much less than that of the storm canopy, cloud top temperature was weakly, but consistently, inversely related to rainrate. At a scale of about 50 km rainrate proved to be positively related to the standard deviation of temperature. These results suggest that in a thresholded infrared image there is information on rainrate. This information lies in temperature itself and in certain simple measures of the variation of temperature. Still to be established is the degree to which the temperature and variation of temperature information is independent.

ACKNOWLEDGMENTS

I would like to thank Barry Hinton for discussions through the course of this project and Brian Auvine as well as Dr. Hinton for a thoughtful review of this report. Thanks also are extended to Angela Crowell and Jody Edwards, who typed the text.

TABLE OF CONTENTS

1. Introduction

The discovery of ice-layer scattering in the 37 GHz window region of the microwave spectrum (Spencer et al., 1983; Grody, 1984) has brightened prospects for using microwave radiometers on satellites to measure convective rain over land. Recently, for example, Spencer (1984) described a multichannel algorithm which was able to explain two-thirds of the variance in a large sample of radar rainrates averaged over areas 20 km on a side. With such an algorithm the observations of a single instrument like the Scanning Multichannel Microwave Radiometer (SMMR - see Njoku et al., 1980) would be sufficient to provide snapshots of rainrate at intervals of one-half to two or more days.

This is an impressive achievement, but for purposes of monitoring rainfall over croplands it falls short of solving the problem. Enthusiasm for satellite microwave radiometers as instruments to measure rain over land is tempered by the realization that, however well the instruments may perform, the satellites of today and of the near future simply cannot provide enough observations to adequately measure accumulations of rain over periods shorter than a week (Atlas and Thiele, 1982; Barrett and Martin, 1981). If this scale of rainfall is to be addressed by means of satellites, microwave observations must be supplemented. In tropical and near-tropical latitudes the most obvious source of supplemental observations is the infrared channel on geostationary satellites.

Techniques for inferring rainrate from satellite infrared images have been summarized elsewhere (e.g., see Barrett and Martin, 1981; Atlas and Thiele, 1981). It is sufficient here to say that all depend mainly on equivalent black body temperature (T), which (typically) is thresholded, and that all suffer, first, from an inability consistently to distinguish

detached cirrus cloud from cumulonimbus anvil cloud and, second, from an inability to tell where, within an anvil canopy, rain may be falling. Here we report on an attempt to relate rainrate to structure in infrared cloud top temperature.

One case is treated, the Ozark storm of 23 June 1979. Raingauge, radar, microwave and some infrared aspects of this storm were described by Martin (1985). Briefly, the Ozark storm was a complex of cumulonimbus clouds whose clumped towers over the two hours of observation fed, lifted and occasionally penetrated the top of a large oval canopy of outflow cirrus cloud (Fig. 1). Echoes observed by the Monett, MO radar formed four groups (Fig. 2). Three of the four echo groups (K1, M1 and O1) each corresponded to a cold event[1] in SMMR 37 GHz brightness temperatures (E2, E1 and E3, respectively). The fourth echo group (K2) corresponded to a west-pointing spur off cold event E1. Three reports of severe weather -- including a flash flood -- were uncovered for echo group O1; a heavy rain report (up to 8 inches) for M1. Finally, the extreme cold event -- E1 -- was found to be associated with the coldest of the canopy's cloud-top temperatures and the largest of the two most intense echo groups.

2. Classification of Temperature Structure

An attempt was made to isolate the primary scale of structure internal to the canopy. Four contiguous scales were defined (Fig. 1). These scales cover the interval from 20 km to 400 km, roughly in increments of factor

---

[1]"Cold event" is defined as a group of cold (relative to typical ambient values) 37 GHz brightness temperatures which cannot be explained in terms of a lake, bay or other body of water.

two. A set of classification rules also was defined. The rules define a "cloud" as a center of brightness (i.e., cold spot) which (a) consists of at least three pixels and (b) is well separated in distance or brightness from its nearest neighbor. Each cloud so defined was given a number. At any particular scale there might be one cloud, several clouds or none at all. Smaller clouds could be nested inside larger clouds and continuity in clouds was to be preserved from one image to the next. The reader is referred to the appendix for more information on the classification rules.

By means of acetate overlays, the classification was applied to a five-image sequence which at one-half hour resolution covered the period from 0000 to 0200 (all times in this paper are Central Standard). An MB enhancement (Corbell et al., 1979) had been applied to each of the images. We believe the results would have been similar with any linear enhancement of the cold end of the infrared temperature interval.

A sample cloud map is shown as Fig. 3. From the cloud maps a block diagram (not shown) was drawn which depicts the rank (i.e., hierarchical) structure of all the clouds and their persistence. At the C-scale (25 to 50 km) and larger generally there was good time continuity. There may have been a slight preference for the B-scale (50-100 km). It was hard at times to judge whether a feature was revitalized or new. Mergers also were troublesome. These two problems came up most often in a cold cloud of B-scale which lay over and northwest of Monett (Fig. 3).

In terms of numbers of clouds, conditions were nearly steady through 0030 (Fig. 4). Thereafter the number of small clouds (C- and D-scale) dropped by almost half. By 0100 D-scale clouds were present only within the B-scale cloud due north of Monett.

Drawing particularly from the work of Griffith et al. (1978), Stout et al. (1979), Negri and Adler (1981), and Adler and Mack (1984), for the present case we might expect that at least the echo groups would be reflected in the clouds as those clouds have been classified above.

In Fig. 5 the echo group boundaries for radar time 0035 have been overlaid on the 0300 infrared image. For the Oklahoma echo group, which was of the character of a cell, the match is good. For the Kansas and Missouri echo groups the match is only fair. One cloud, the cloud closest to Monett, lies for the most part outside the echo group boundaries.

In Fig. 6, for the same times the cloud boundaries have been overlaid on the radar rain image. If we think of K2 (see Fig. 2) as consisting of two raincells at this time, each of the five largest raincells is fairly well bounded by a cloud outline; moreover, the easternmost clump of three primary raincells itself is bounded by a cloud outline. However, D-scale clouds (20-50 km) show no particular match to small raincells and for several clouds (e.g., 5(B), 3(B), and 16(C)) there simply are no raincells at all.

3. Temperature versus Rainrate

Within echo groups, the relationship between rainrate and temperature also was examined on a pixel-by-pixel basis. It was convenient in the present case to work with pixels 4 km on a side, even though the radar images had been digitized at 10 km resolution. The 0030 infrared image (with a scan time at Monett of 0034) was compared with the 0035 radar image. This comparison was accomplished using the Man-computer Interactive Data Access System (McIDAS; Suomi et al., 1983), as follows. For each echo group boundary a window was made which (a) was entirely contained within

the digitized part of the radar rain image and (b) as nearly as possible was equivalent in shape and area to the echo group boundary. Each window (or grid element, Fig. 7) isolated paired arrays of infrared temperature and radar rainrate. From these paired arrays scatterplots were made, with rainrate as the abscissa (Fig. 8).

Plotted in this form the points have a characteristic "anvil" distribution: large scatter at low rain rates; small scatter at high rain rates; and a ceiling on the cold-temperature side of the distribution. Thus, in every case there is a tendency for the modal (and, presumably, mean) value of cloud-top temperature to decrease as rain rate increases. At 0035 echo group K2 was producing the heaviest rain. The system (M1) associated with the extreme cold event was distinctive for the sharpness of its "anvil".

4. Variance of Temperature

In the context of infrared images only infrequently is texture invoked to help estimate rain. Texture has been ignored partly because temperature gradients at the edges of clouds usually swamp the inner gradients which may be associated with rain (e.g., see Coakley, 1983).

Until very recently the infrared rain estimation techniques which do employ texture have tended to be manual or at least interactive (e.g., Scofield and Oliver, 1977; Barrett, 1980; Martin and Howland, 1985). In such techniques cloud-edge gradients can usually be identified and discounted. Then rain is favored in those parts of the cloud which are strongly textured; that is to say (in the case of infrared), where the top of the cloud carries turrets and domes or is otherwise roughened.

Recently three studies have sought to measure the rain information contained in infrared texture. In two of these three studies statistical pattern recognition was applied to geostationary satellite infrared images. Lee et al. (1984), finding no rain information in infrared texture, suggested that their classification window was too small in relation to the resolution of the infrared images. This result prompted Wu et al. (1985) to try a classification window two and one-half times wider and longer (20 km by 20 km). With the larger window several related measures of texture proved to be helpful in a rain/no rain classification of window scenes.

The third study also is statistical, but less complex in its design than either of the pattern recognition studies and more extensive in its data base. Paul (1983) compared GOES-East infrared temperature with station observations of clouds and rain. Her study covered August 1979 daytime reports from National Weather Service stations along the U.S. Gulf of Mexico and central Atlantic coasts. For each station at each hour the standard deviation of temperature (S_T) was calculated for each of four windows centered on the station. The smallest of these windows, at 4 by 4 pixels (about 28 km on a side), was slightly larger than the window used by Wu et al. By means of the station reports Paul classified the window standard deviations as (1) overcast and broken,[2] (2) overcast only and (3) rain only. Each of these three classes was, in turn, divided into subclasses: rain and no-rain in the case of the first two; light rain and moderate or heavy rain in the case of the third. For each subclass Paul

---

[2]Paul (1983) defined "broken" as five-eights to seven-eights cloud cover at a low, middle or high level, or some combination of levels, and no overcast at any level.

calculated both the mean and standard deviation of S_T. Her results for the 10 by 10 window are plotted in Fig. 9.

There is a large overlap in the standard deviations of S_T and only a small difference between the means of S_T for the rain class. Nevertheless, within each of the three classes the means conform to the expected pattern: lower for no-rain (or light rain, in the case of the third class). Paul found a somewhat weaker, although otherwise similar, relationship for S_T calculated from 4 by 4 pixel windows. She concluded that in the presence of clouds the standard deviation of temperature can help to isolate areas of rain.

I measured S_T inside an isotherm -- 234 K -- which was chosen to mark the edge of the 23 June 1979 canopy. In one trial -- called best-choice -- I measured S_T in windows which were either centered on heavy rain or altogether outside any rain. In another trial -- called rain-independent -- I measured S_T with no regard to the distribution of rain (as observed by the Monett radar).

In both trials as nearly as possible the windows were positioned entirely within the region for which the canopy (as defined by the 234 K isotherm) overlapped the part of the radar ppi which had been digitized earlier. Measurements were made for two infrared/radar image pairs, 0030/0035 and 0100/0059. These pairs are not distinguished in the plots which follow. The measurements included (from the infrared images) window-mean temperature and (from the radar-rain images) window-mean rainrate.

For the best-choice trial the window was one-half degree in latitude and longitude. With the radar-rain images as guides, windows of this size were placed over each of the five foremost rain centers. For each

rain-center window one or more windows of the same size also were placed in nearby rainless areas of the canopy. All the windows are shown in Fig. 10.

In Fig. 11, for each window the mean of rainrate is plotted against S_T. As expected, in terms of rainrate, the points fall into two distinct groups. Significantly, the points also tend to cluster in terms of S_T. Thus, in spite of a large range, the wet points reflect significantly higher values of S_T than do the dry points.

The rain-independent trial is a more critical test of rain-information contained in S_T. In this trial a window one degree in latitude and longitude was stepped around the ppi annulus such that successive windows were just adjacent to each other. The windows are shown in Fig. 12.

Standard deviation of temperature for the rain-independent trial is plotted against mean rainrate in Fig. 13. There is a wide range in values of S_T near the zero end of the rainscale. Otherwise, the distribution of points suggests a minimum near 5 mm h^{-1}. A low-rain-rate minimum would be consistent with Fig. 11.

Is rainrate also related to mean temperature? For the best-choice trial, mean temperature is plotted against mean rainrate in Fig. 14. The best-fit line carries a marked negative slope. For the rain-independent trial, mean temperature is plotted against mean rainrate in Fig. 15. Again, the best-fit time line carries a negative slope. Noted in passing is the 220 K intercept of both the best-fit lines. This is much colder than the temperatures which commonly are used as thresholds for infrared rain estimation.[3]

---

[3]In a day's sample of growing cumulonimbi, Negri and Adler (1981)
(Footnote Continued)

The behavior of points in both figures is consistent with the "anvils" which were prominent in scatterplots of pixel temperatures and rainrates (see Fig. 8). More significantly, taken together with Figures 11 and 12, it suggests that S_T also is correlated with mean temperature.

The relationship of S_T to mean temperature is plotted for the best-choice trial in Fig. 16. The points fall into two groups, one group on either side of the 212 K line. With one exception the points are divided as well by wet and dry; moreover, the wet (rain center) points do tend to have lower mean temperatures as well as larger standard deviations. For this set of points the correlation, -0.4, is a substantial fraction of the individual correlations of mean rainrate with mean temperature and S_T.

In Fig. 17 for each window of the rain-independent trial the mean of temperature is plotted against S_T. Except in two respects the distribution of points is like that of Fig 11. The first discrepancy is the upward-pointing tail at temperatures warmer than 220 K. This tail probably is due to encroachment of two windows (those to the east and southeast of Monett) on the edge of the canopy. The second discrepancy is the absence of a low-temperature rise in S_T. Apparently this is due to averaging.

5. Difference Image

We saw in Section 2 a scale-dependent contrast in infrared clouds: large clouds were persistent; small clouds were transient; and the

---

(Footnote Continued)
found 229 K to be the coldest cloud top minimum temperature marking the onset of rain. The coldest temperature Lovejoy and Austin (1979) used to delineate rain was 232 K. Stout et al. (1979) used a temperature of 247 K to define rain-cloud area; cloud area in the technique of Griffith et al. (1978) [and in the simplified version of Negri and Adler (1984)] is defined by the 253 K isotherm. Scofield and Oliver's (1977) range of contoured temperature intervals begins (on the warm side) at 240 K.

intermediate- to small-sized clouds were most closely associated with raincells. There is a large body of experience that associates rapid cooling with thunderstorms (e.g., Scofield and Oliver (1977) and Negri and Adler (1981)). Thus we might expect to find a rain signature in the difference between two consecutive infrared images and we might expect that signature to be strongest on the scale of intermediate- to small-sized clouds.

A difference image (Fig. 18) was created by subtracting (on McIDAS) the 0030 image from the 0100 image and adding an offset. Amplitude in such an image is the simplest possible temporal analog to texture in an ordinary image.

This difference image emphasizes large and small scales at the expense of the intermediate scale. Facing crescents of opposite tone define the very large-scale. They mainly reflect the eastward movement of the canopy. Between the crescents there is much fine structure. Some of this fine structure consists of distinct light and dark cells. These cells tend to be paired and the pairs tend to be clustered. One cluster lies in northeast Oklahoma, astride the 220 km range circle; clearly it is associated with echo group 01 (See Fig. 2). The second cluster lies mainly in southwest Missouri. As part of this cluster seven cells form a string extending from the Kansas-Missouri border eastward some 140 km. As a glance at Fig. 2 will confirm, this string coincides with the axis of the M1/K2 echo group. Remarkably enough, at its western end the spacing of like cells along the string matches the spacing of raincells along the axis of the echo groups.

6. Conclusions

This study has addressed the question of whether structure in cloud top temperature, as that structure is observed by a satellite, might contain unique information on rain within thunderstorms. For the large Ozark storm complex of 23 June 1979, the match of cloud structure to rain rate began to show promise at a scale of about 50 km. At scales larger than 50 km, but still much less than that of the storm canopy, cloud top temperature was weakly, but consistently, (inversely) related to rainrate. The relationship was strongest for the system which produced the most extreme cold event in 37 GHz SMMR observations. It held whether structure was defined in terms of rainrate or in terms of temperature.

In this case, too, within the canopy and at a scale of about 50 km, rainrate proved to be related in a positive sense to a simple measure of texture, the standard deviation of temperature. Although the sample tested here is small, this particular conclusion is supported by two recent statistical studies of much broader scope. If texture is not too highly correlated with temperature, it may be that a simple measure of texture, employed in tandem with a parameter for identifying clouds, might usefully supplement temperature as a measure of rainrate. The strength of the texture-temperature correlation needs to be established. Also needing study is the possibility of gathering additional rain information by measuring small-scale structure in the difference between two consecutive infrared images.

8/DM11/01/ 6

REFERENCES

Adler, R.F., and R.A. Mack, 1984: Thunderstorm cloud height-rainfall rate relations for use with satellite rainfall estimation techniques. J. Clim. Appl. Meteor., 23, 280-296.

Atlas, D., and O. Thiele, 1982: Precipitation Measurements from Space: Workshop summary. Bull. Amer. Meteor. Soc., 63, 59-63.

Barrett, E.C., 1980: The use of satellite imagery in operational rainfall monitoring in developing countries. In (COSPAR) The Contribution of Space Observations to Water Resources Management (V.V. Salomonson and P.D. Bhavsar, Eds.). Pergamon Press, 163-178.

Barrett, E.C., and D.W. Martin, 1981: The Use of Satellite Data in Rainfall Monitoring. Academic Press, London, 352 pp.

Coakley, J.A., Jr., 1983: Properties of multilayered cloud systems from satellite imagery. J. Geophys. Res., 88 (No. C15), 10,818-10,828.

Griffith, C.G., W.L. Woodley, P.G. Grube, D.W. Martin, J. Stout, and D.N. Sikdar, 1978: Rain estimation from geosynchronous satellite imagery - visible and infrared studies. Mon. Wea. Rev., 106, 1153-1171.

Grody, N.C., 1984: Precipitation monitoring over land from satellites by microwave radiometry. Proceedings of IGARSS 1984 Symposium (Strasbourg, 27-30 August 1984; Ref. ESA SP-215), 417-422.

Lovejoy, S., and G.L. Austin, 1979: The delineation of rain areas from visible and IR satellite data for GATE and mid-latitudes. Atmosphere-Oceans, 17, 77-92.

Martin, D.W., 1985: Satellite Microwave Observations of a Storm Complex: A Comparative Analysis. Space Science and Engineering Center, University of Wisconsin-Madison.

Martin, D.W., and M.R. Howland, 1985: Grid history: A geostationary satellite technique for estimating daily rainfall in the tropics. J. Clim. Appl. Meteor, in press.

Negri, A.J., and R.F. Adler, 1981: Relation of satellite-based thunderstorm intensity to radar-estimated rainfall. J. Appl. Meteor., 20, 288-300.

Negri, A.J., and R.F. Adler, 1984: A new technique to infer convective rainfall from satellite infrared cloud observations. Preprints: Conference on Satellite/Remote Sensing and Applications. (Clearwater, Beach, FL, 25-29 June 1984). American Meteorological Society, Boston, 58-63.

Njoku, E.G., J.M. Stacey, and F.T. Barath, 1980: The Seasat Scanning Multichannel Microwave Radiometer (SMMR): Instrument description and performance. IEEE J. Oceanic Engr., OE-5, 100-115.

Paul, L.S., 1983: A Study of Precipitation Occurrence Using Visual and Infrared Satellite Data. Master's Thesis, Naval Postgraduate School, Monterey, CA, 114 pp.

Scofield, R.A., and V.J. Oliver, 1977: A Scheme for Estimating Convective Rainfall from Satellite Imagery. NOAA Tech. Memo. NESS 86, Washington, D.C., 47 pp.

Spencer, R.W., 1984: Satellite passive microwave rain rate measurement over croplands during spring, summer, and fall. J. Clim. Appl. Meteor., 23, 1553-1562.

Spencer, R.W., W. Olson, R. Wu, D.W. Martin, and J.A. Weinman, 1983: Heavy thunderstorms observed over land by the Nimbus 7 Scanning Multichannel Microwave Radiometer. J. Clim. Appl. Meteor., 22, 1041-1046.

Stout, J.E., D.W. Martin, and D.N. Sikdar, 1979: Estimating GATE rainfall with geosynchronous satellite images. Mon. Wea. Rev., 107, 585-598.

Suomi, V.E., R. Fox, S.S. Limaye, and W.L. Smith, 1983: McIDAS III: A modern interactive data access and analysis system. J. Appl. Meteor., 22, 766-778.

Wu, R., J.A. Weinman, and R.T. Chin, 1985: Determination of rainfall rates from GOES satellite images by a pattern recognition technique. J. Ocean. Atmos. Technol. In press.

CAPTIONS

Fig. 1. GOES-East infrared image for 0030 on 23 June. A location correction for perspective (see Martin, 1985) has been applied to this image. The cross marks the location of the Monett, MO radar in relation to the perspective-corrected image. Ellipses indicate the four scales of the infrared cloud classification. Diameters are 50, 100, 200 and 400 km for, respectively, scales D, C, B and A.

Fig. 2. Image of radar rainrate at 0035. The crosses mark the 220 km range circle centered on the Monett radar. The radar itself is marked by the two intersecting squares. State boundaries are shown outside the 220 km range circle. The inset indicates echo group boundaries and names.

Fig. 3. Infrared cloud map and enhanced infrared image for 0030. Clouds are numbered and labelled according to scale. Boundaries are drawn in proportion to scale, with the thickest line corresponding to the largest scale.

Fig. 4. Infrared cloud frequency versus time for each of the four scales (A, B, C and D). Image number refers to the infrared sequence (1␣0000, 2␣0030...5␣0200). Frequencies are plotted separately for the two A-scale clouds, 1 and 2.

Fig. 5. Echo group boundaries at 0035 superimposed on the EB-enhanced 0030 infrared image.

Fig. 6. Infrared cloud boundaries at 0030 superimposed on the 0035 radar rainrate image.

Fig. 7. Image of radar rainrate at 0035 with echo group rectangles.

Fig. 8. Scatterplots of temperature versus rainrate for each echo group rectangle. Temperatures are from the 0030 satellite image; rainrates are from the 0035 radar image.

Fig. 9. Standard deviation of satellite infrared temperature (S_T) for three categories of surface station report: overcast and broken (O & B), overcast (O) and rain (R). Overcast and broken and overcast reports are divided into no-rain (left) and rain (right) classes; rain into light (left) and moderate and heavy (right) classes. The mean of S_T for each class is shown by the dot, the standard deviation about the mean by the upright bar. S_T was calculated for a 10 x 10 window. After Paul (1983).

Fig. 10. Best-choice windows for comparisons of temperature variance with rainrate. These windows are shown over the 0030 infrared image, in which temperatures between 231 and 234 K, inclusive, are black. The central cross marks the location of the Monett radar; the ellipse of crosses marks the 220 km range circle.

Fig. 11. Standard deviation of temperature versus mean rainrate for the best-choice windows. Dots represent windows from rain centers, circles represent windows from the rain-free part of the canopy.

Fig. 12. As for Fig. 10, except rain-independent windows.

Fig. 13. Standard deviation of temperature versus rainrate for the rain-independent windows.

Fig. 14. Mean temperature versus mean rainrate for the best-choice windows.

Fig. 15. Mean temperature versus mean rainrate for the rain-independent windows.

Fig. 16. Standard deviation of temperature versus mean temperature for the best-choice windows.

Fig. 17. Standard deviation of temperature versus mean temperature for the rain-independent windows.

Fig. 18. Image created by subtracting 0030 infrared digital counts from 0100 digital counts and adding an offset. The zero-change (constant temperature) level is indicated by the uniform black tone. Tones tending toward white indicate warming; tones tending toward black indicate cooling.

Fig. 19. Schematic profile of brightness illustrating two candidate clouds. Terms are defined in the appendix.

APPENDIX

A System for Classifying and Following Clouds within a Canopy

Here "cloud" is defined as a center of brightness (i.e., cold spot) which a) consists of at least three GOES infrared pixels and b) is well separated in distance or brightness from its neighbors. The idea of separation is illustrated in Fig. 19 which shows brightness across the centers of two cold spots within a thunderstorm canopy. The cold spots are labeled P_1 and P_2, with P_1 assumed to be larger (but not necessarily colder) than P_2. For our purpose the cold spots are defined by six parameters: d_1 and d_2, the diameter of each cold spot; δ, the distance between the coldest pixel of each cold spot; α_1 and α_2, the amplitude of each cold spot; and α_s, the amplitude of the saddle between the cold spots. Amplitude is measured from the background value prevailing just outside the two cold spots. Diameter is measured from the outside edge of the band of gradient which defines a cold spot.

Formally, the separation criterion in distance is met if

$$d_1 \geq 10 \text{ km}$$

and

$$\delta \geq d_1/3.$$

The separation criterion in amplitude is met if the smallest value of (α_1, α_2) is equal to or greater than 5°C and

$$\alpha_s \leq 1/6(\alpha_1 + \alpha_1).$$

Four scales are allowed. In descending order of size these are A, B, C and D. At any particular scale, there may be one cloud, several clouds or none at all.

Every cloud is given a unique "name". The elements of the name allow the cloud to be associated with a particular image. The name tells the

scale of the cloud. For the second and following images, the name also links the cloud to any parent cloud which might have been identified. The "parent" identifier is indispensible in creating cloud life histories.

As a practical matter, in the present case clouds were defined by eye from EB-enhanced hard copy images. No cold spot was considered which was less than two pixels (8 km) from its nearest neighbor. Of those which met this distance criterion, only cold spots which were roughly 30% or more brighter than edge pixels on all sides qualified as clouds. The 30% brightness criterion corresponds roughly to 5°C in temperature.

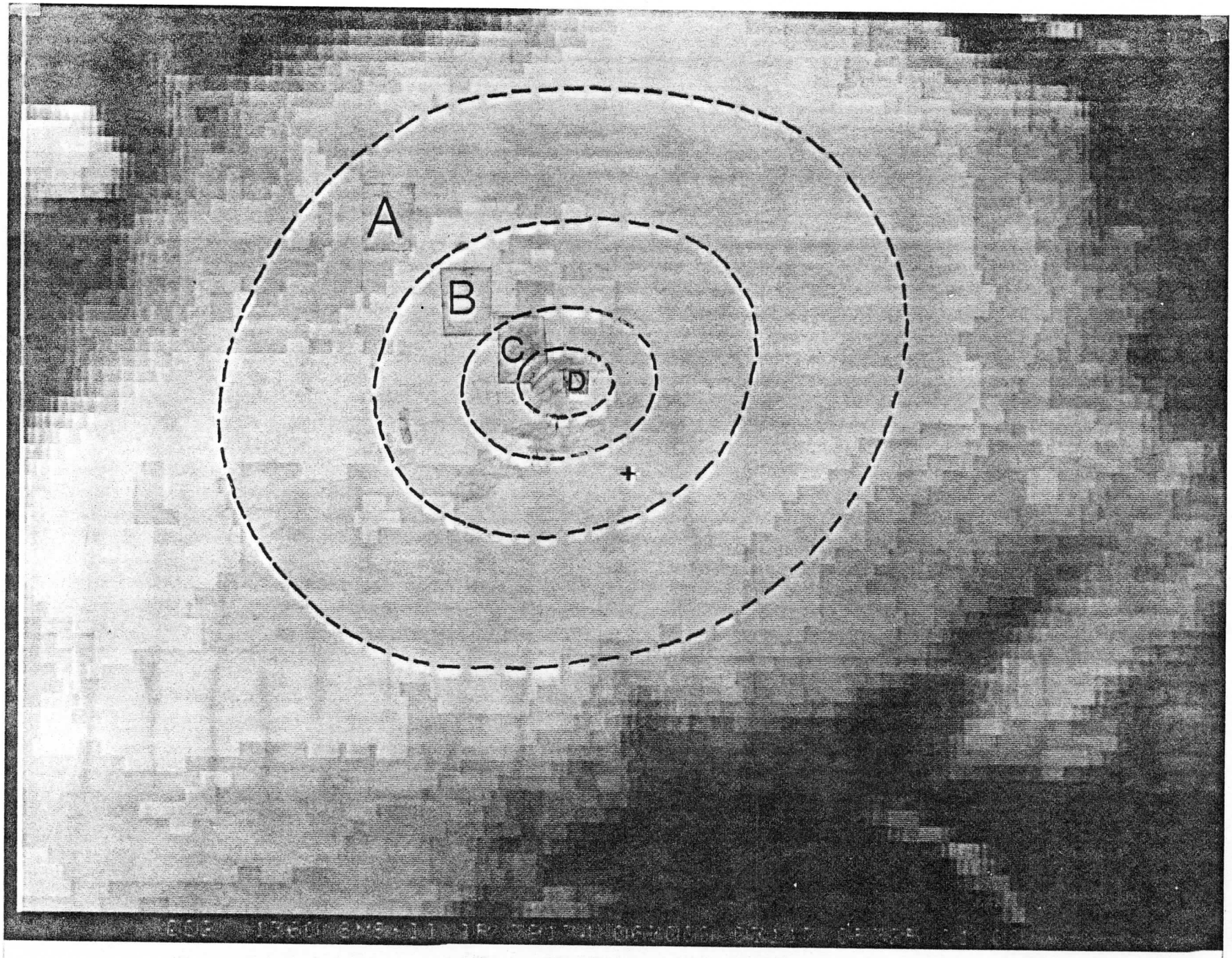

Fig. 1

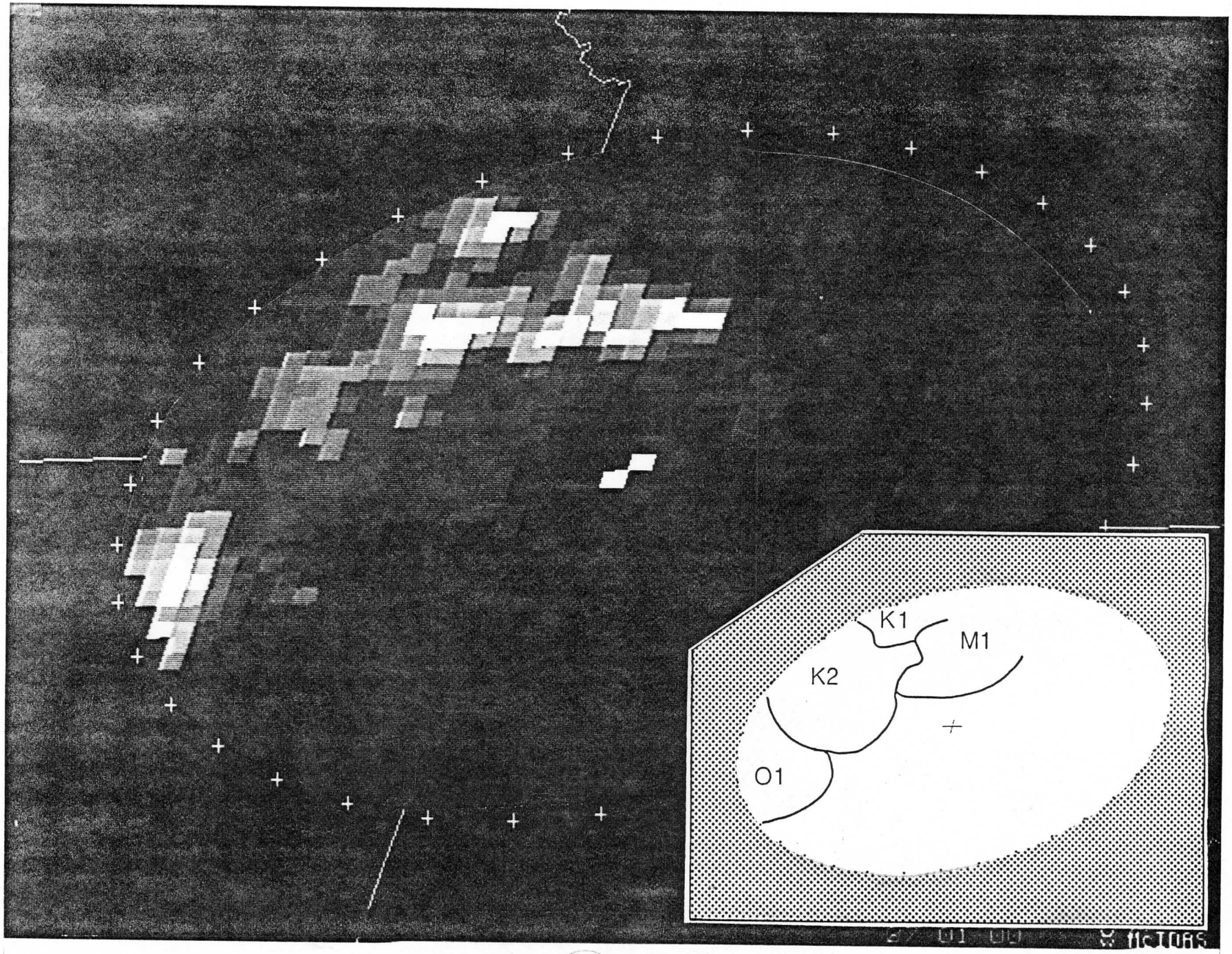

Fig. 2

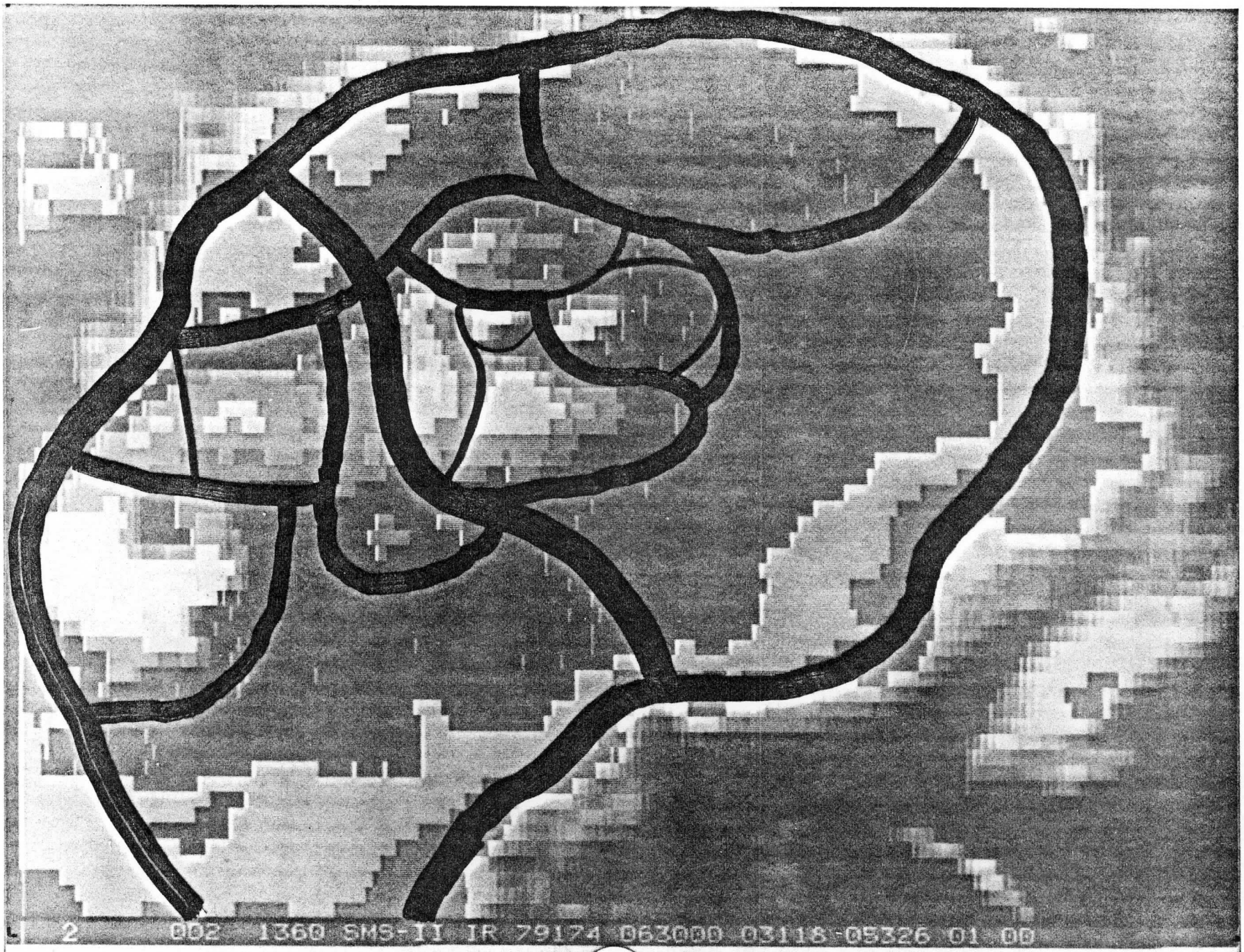

Fig. 3

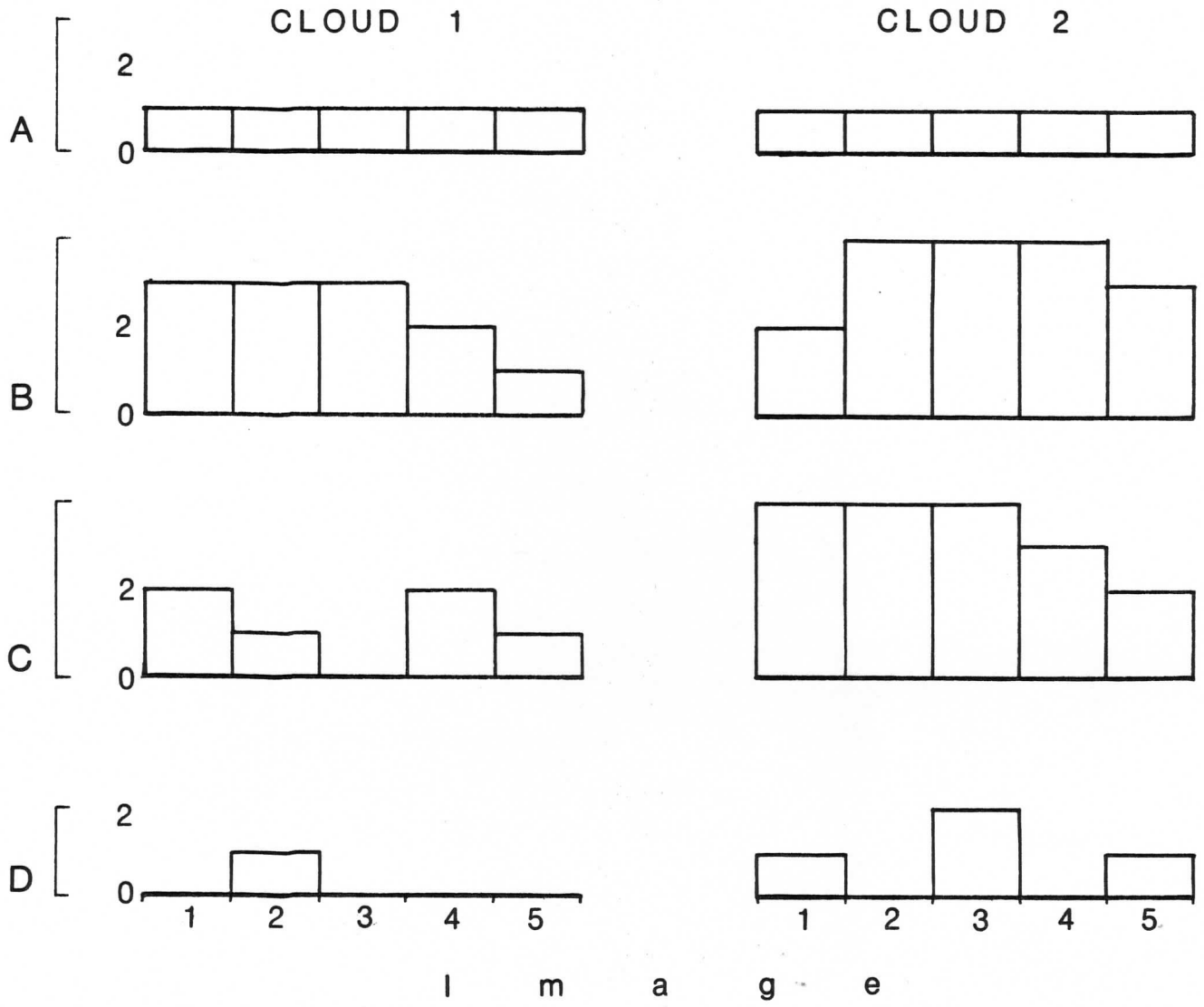

Fig.
4

Fig. 5

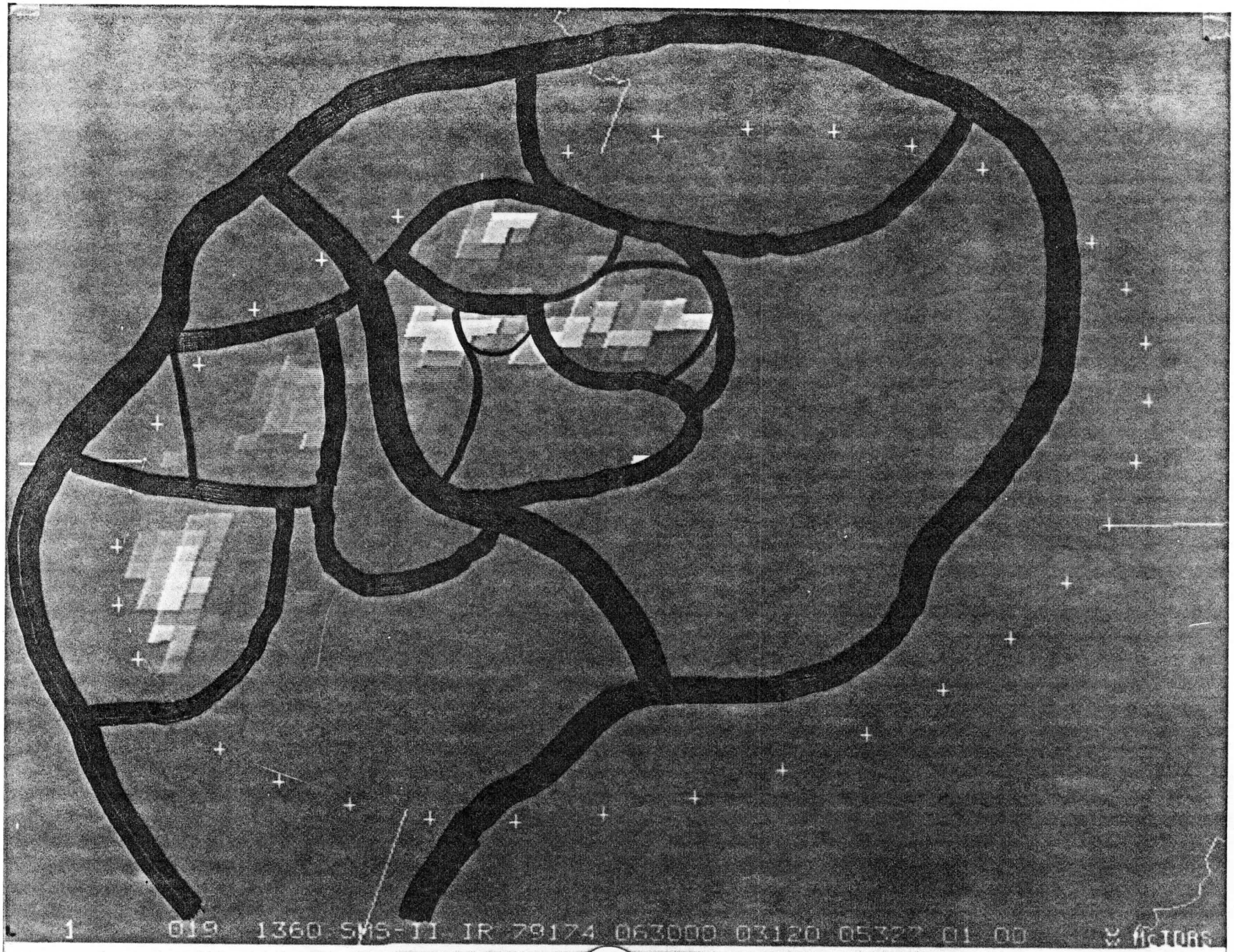

Fig. 6

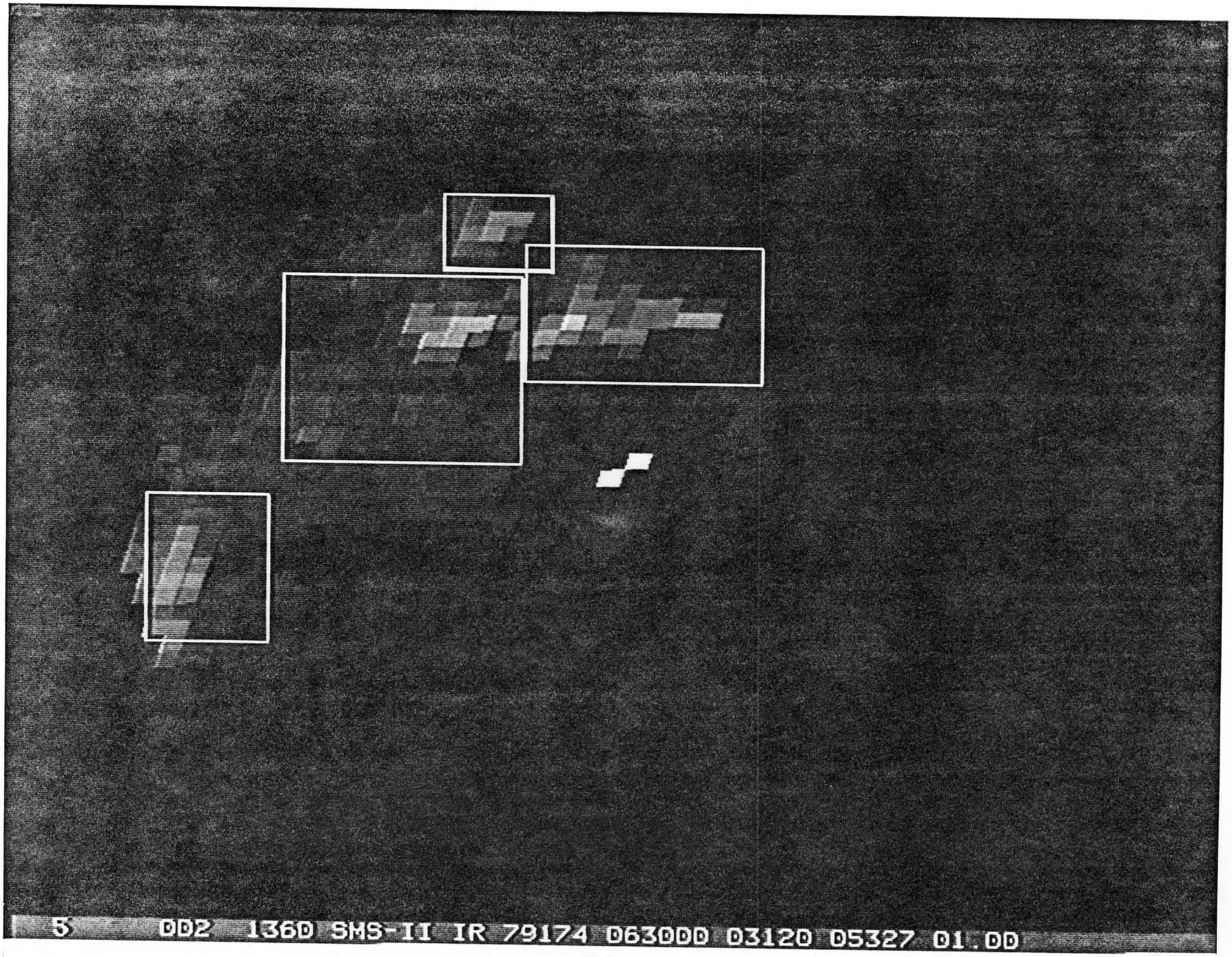

Fig.
7

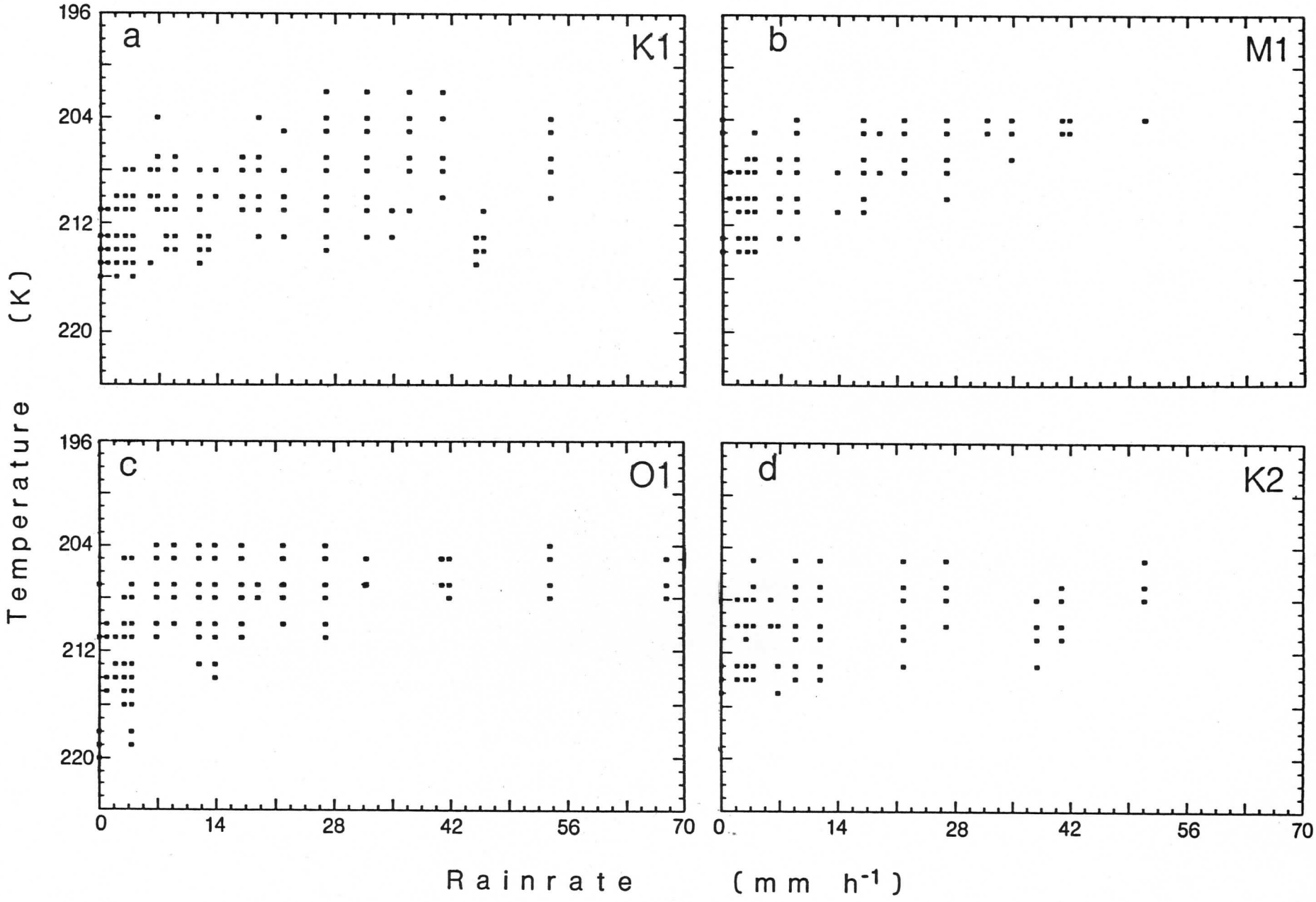
a
K1
b
M1
c
O1
d
K2
196
204
212
220
0
14
28
42
56
70
Temperature (K)
Rainrate (mm h-1)

Fig.
8

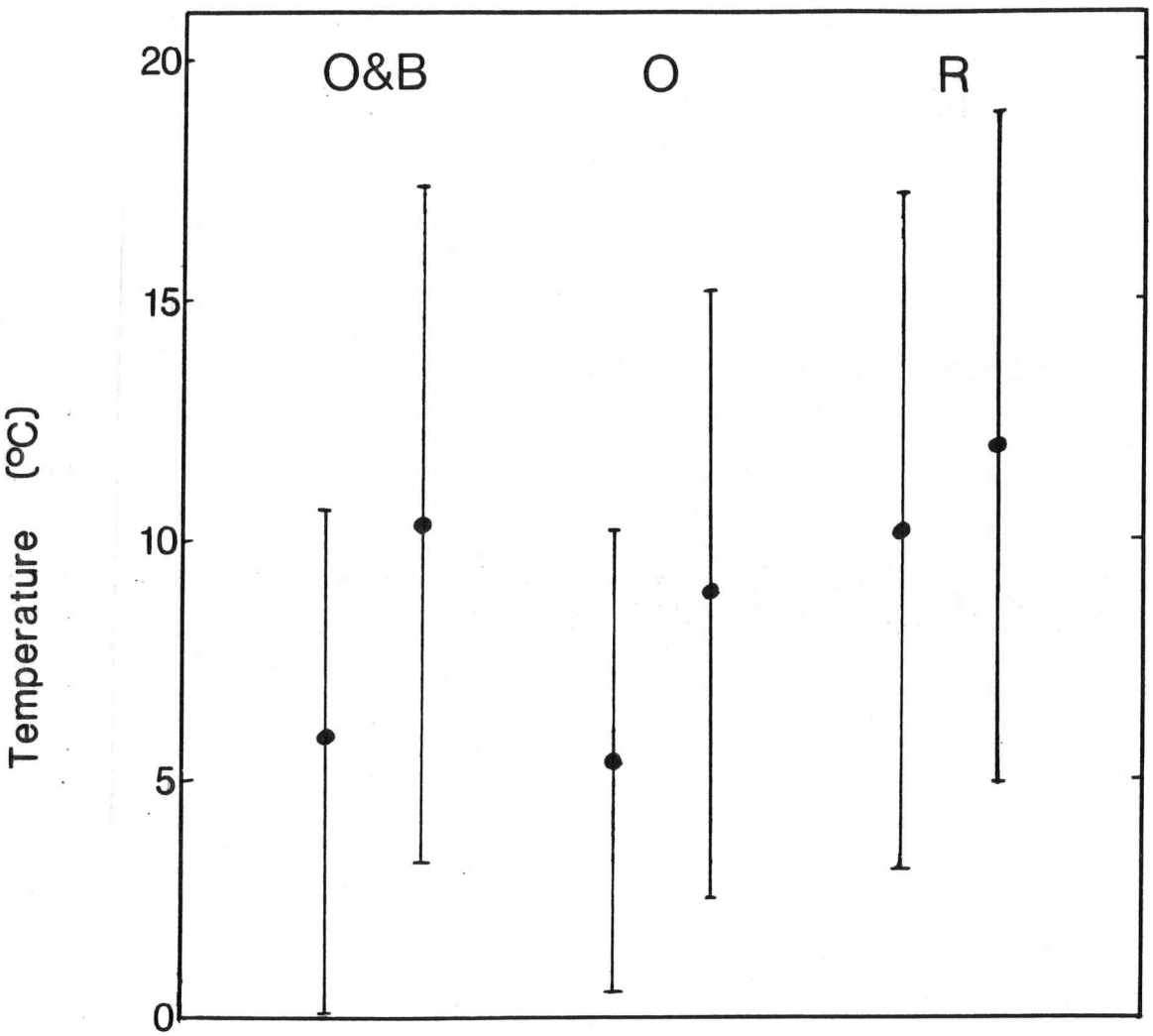

Fig.
9

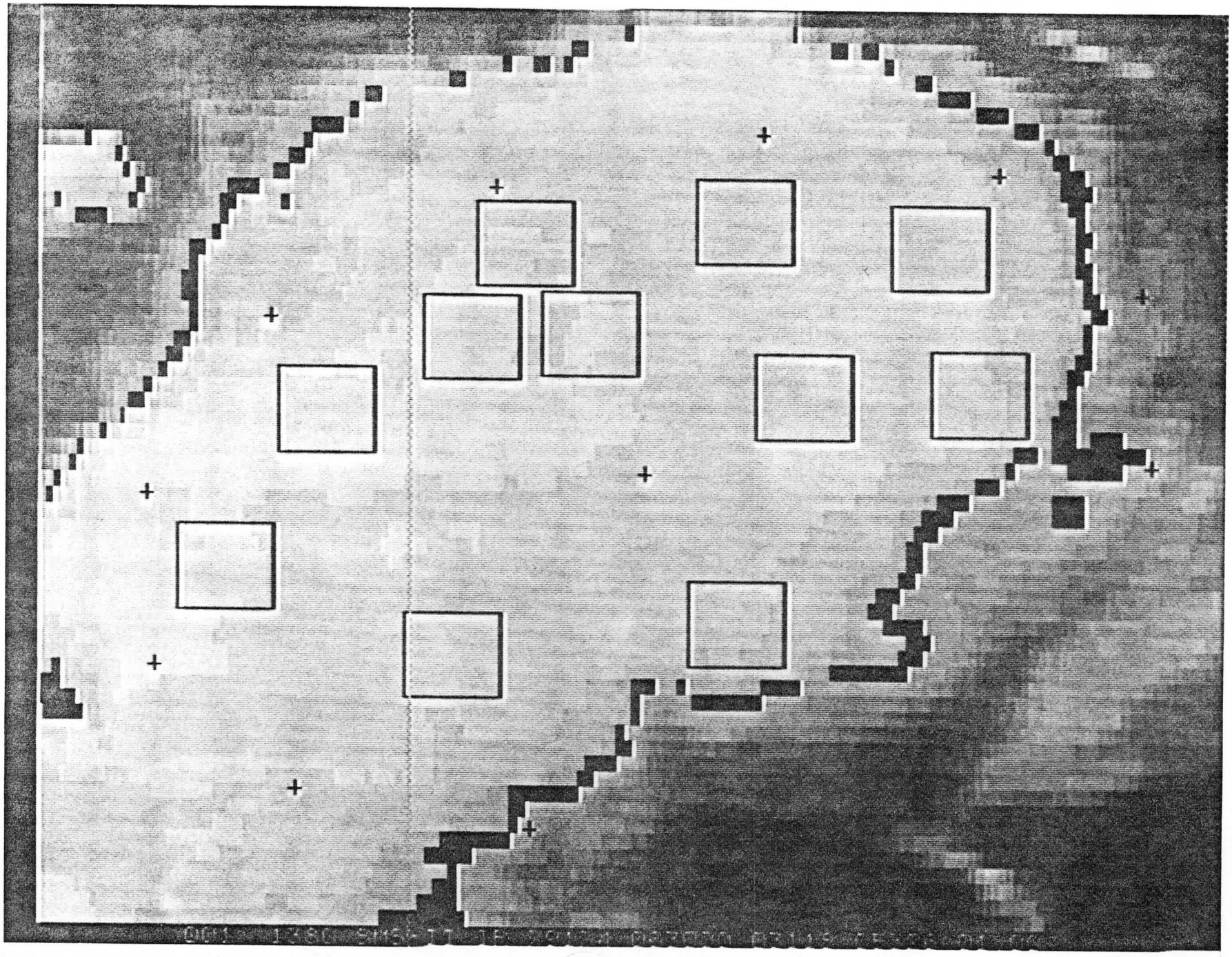

Fig.
10

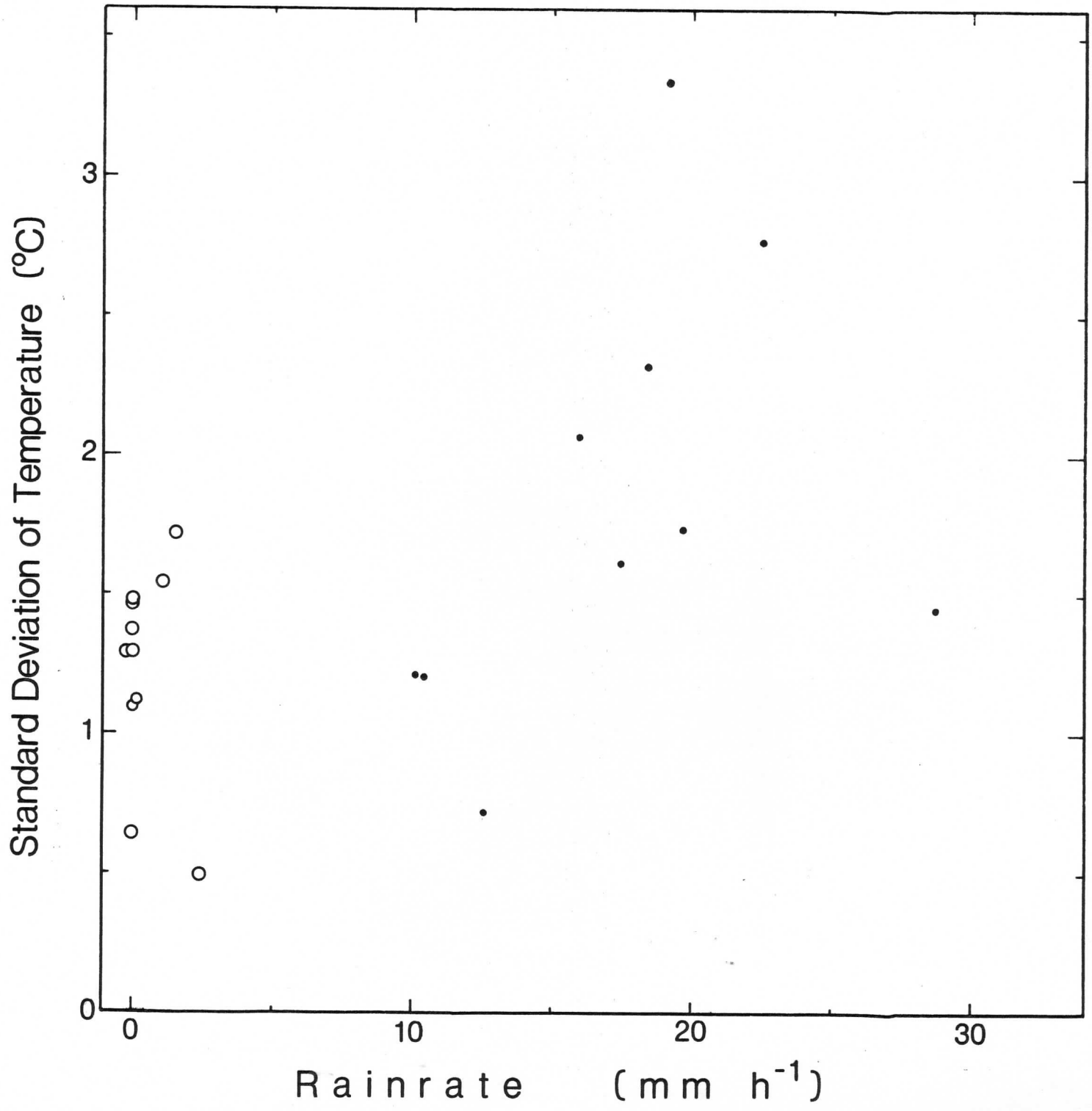
Standard Deviation of Temperature (°C)
0
1
2
3
0
10
20
30
Rainrate (mm h^{-1})

Fig. 11

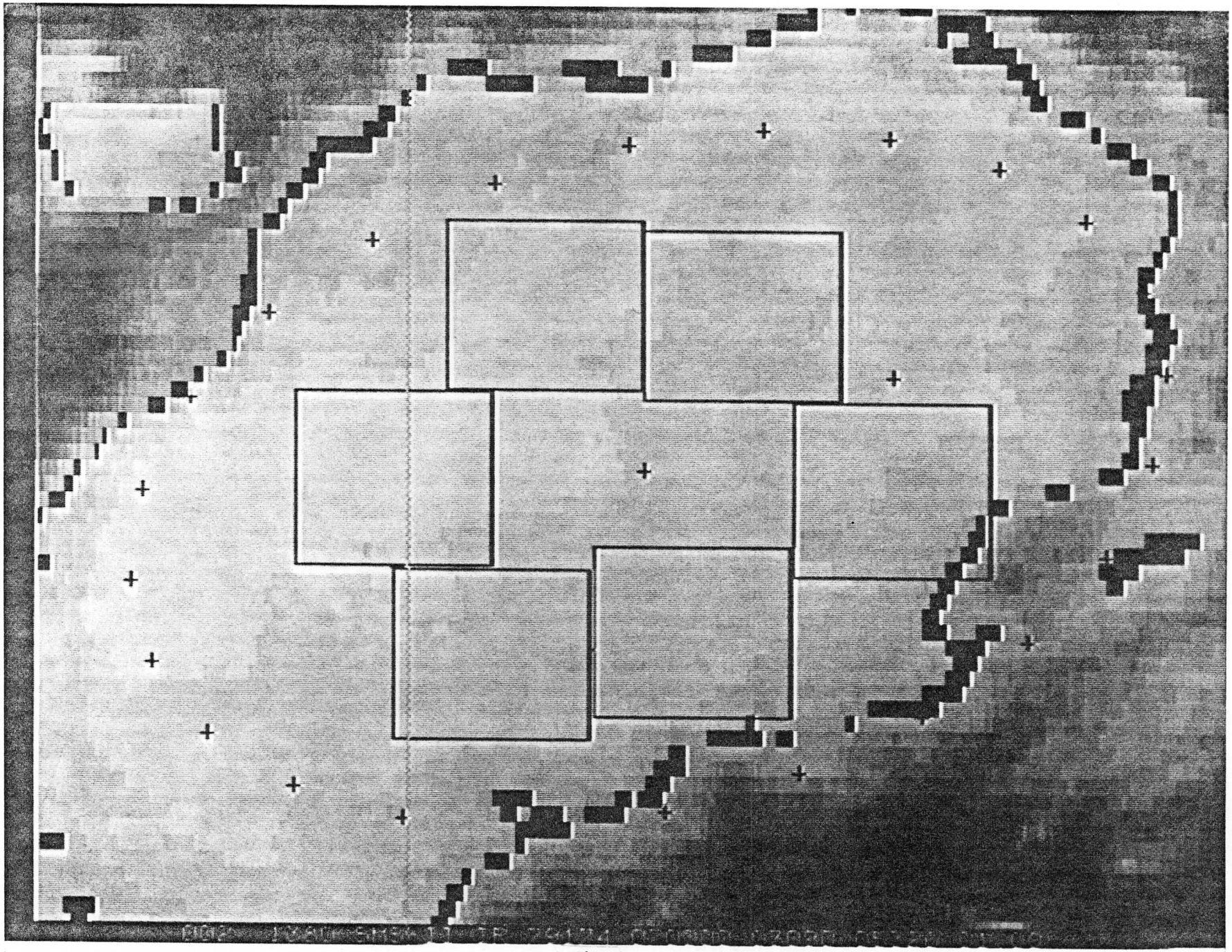

Fig.
12

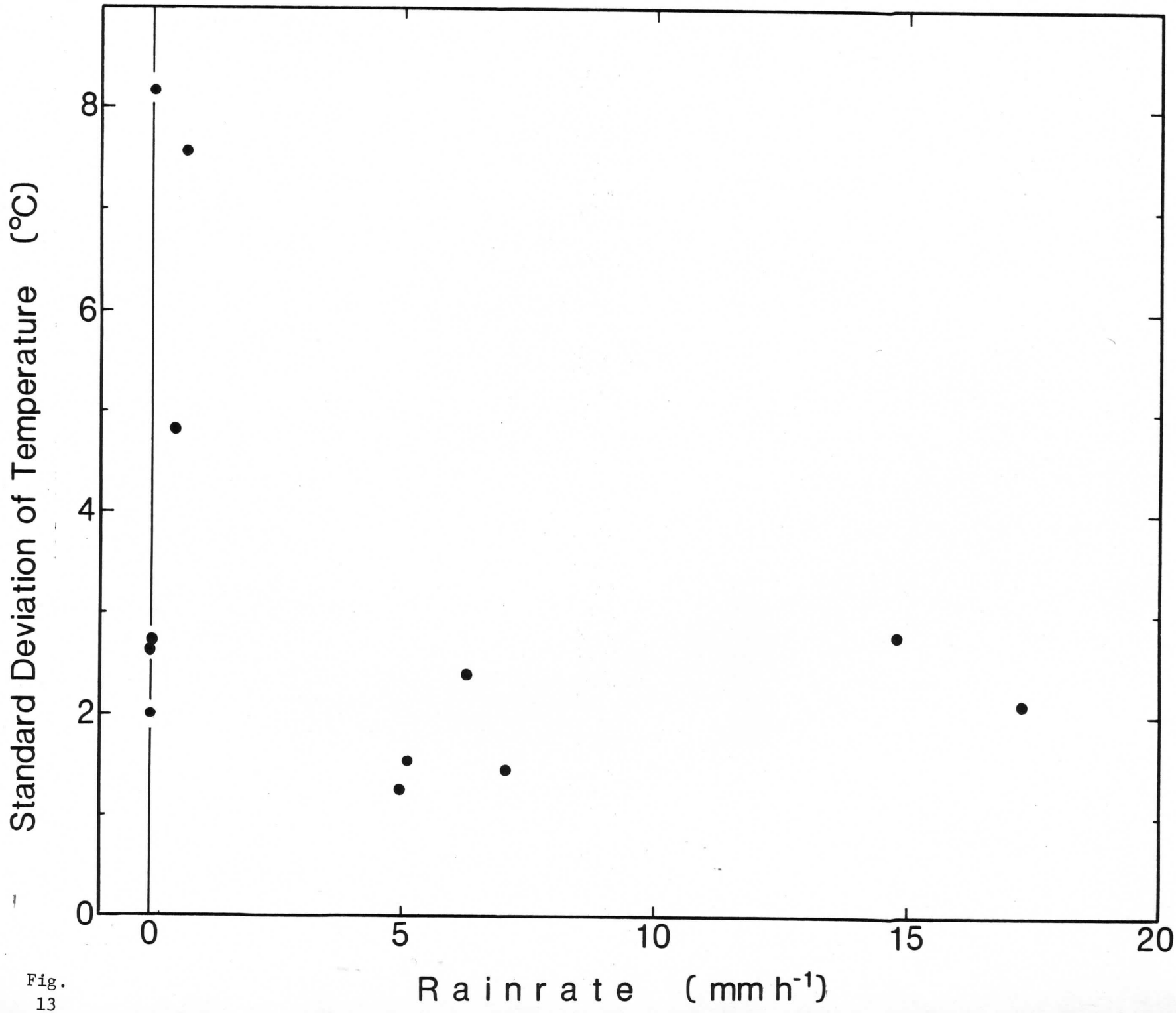
Standard Deviation of Temperature (°C)
0
2
4
6
8
0
5
10
15
20
Rainrate (mm h-1)

Fig. 13

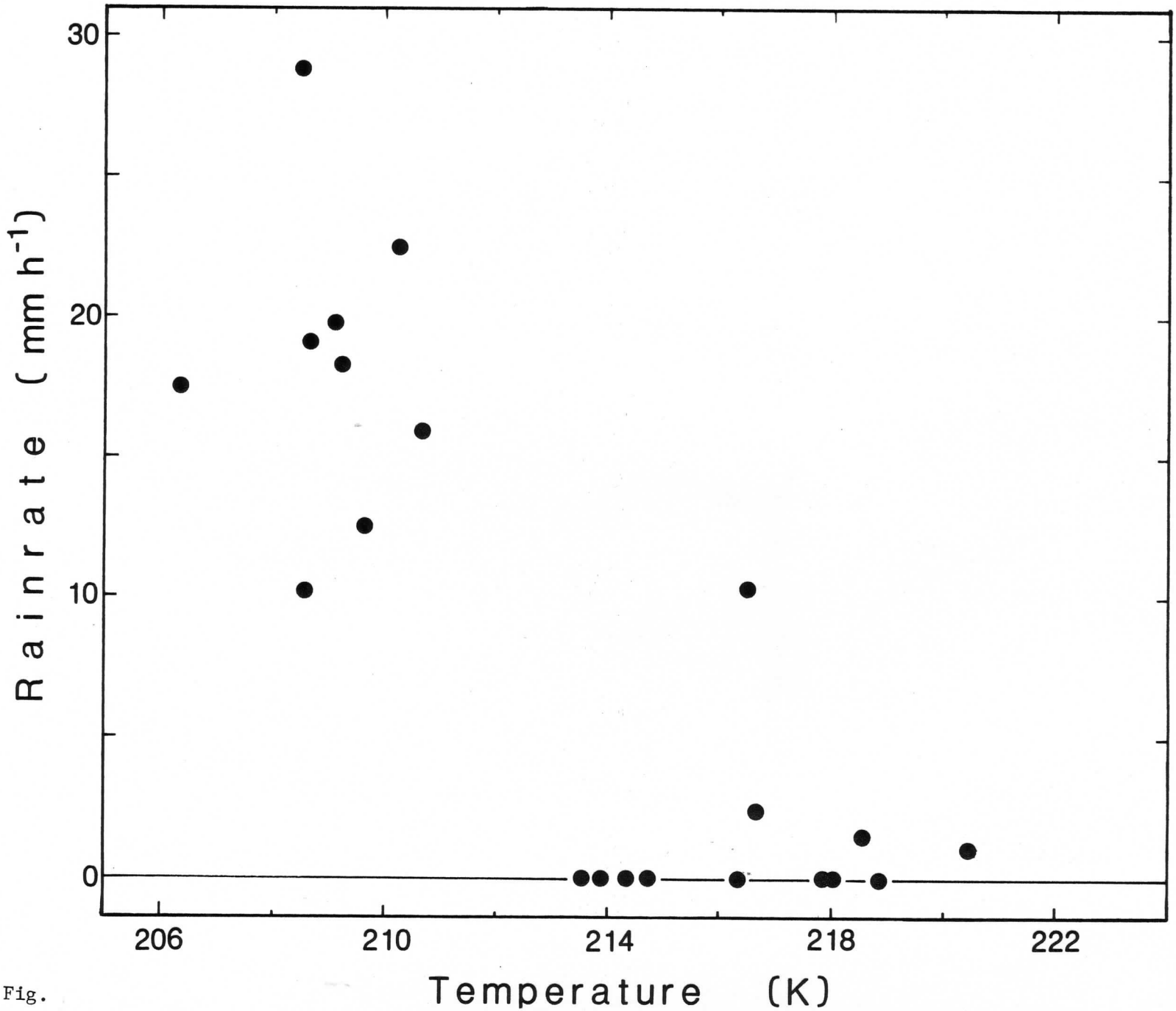

Fig.
14

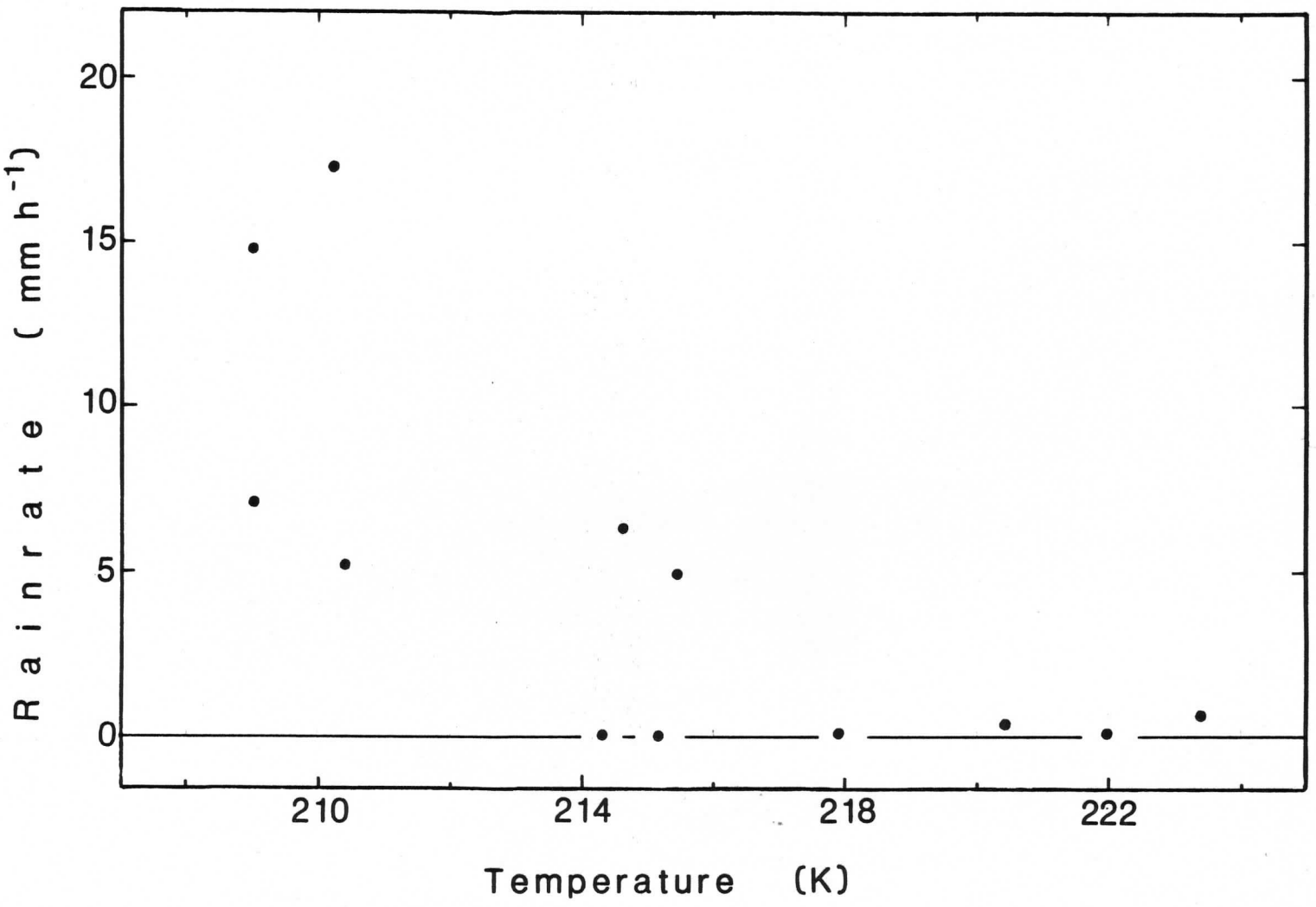

Fig.
15

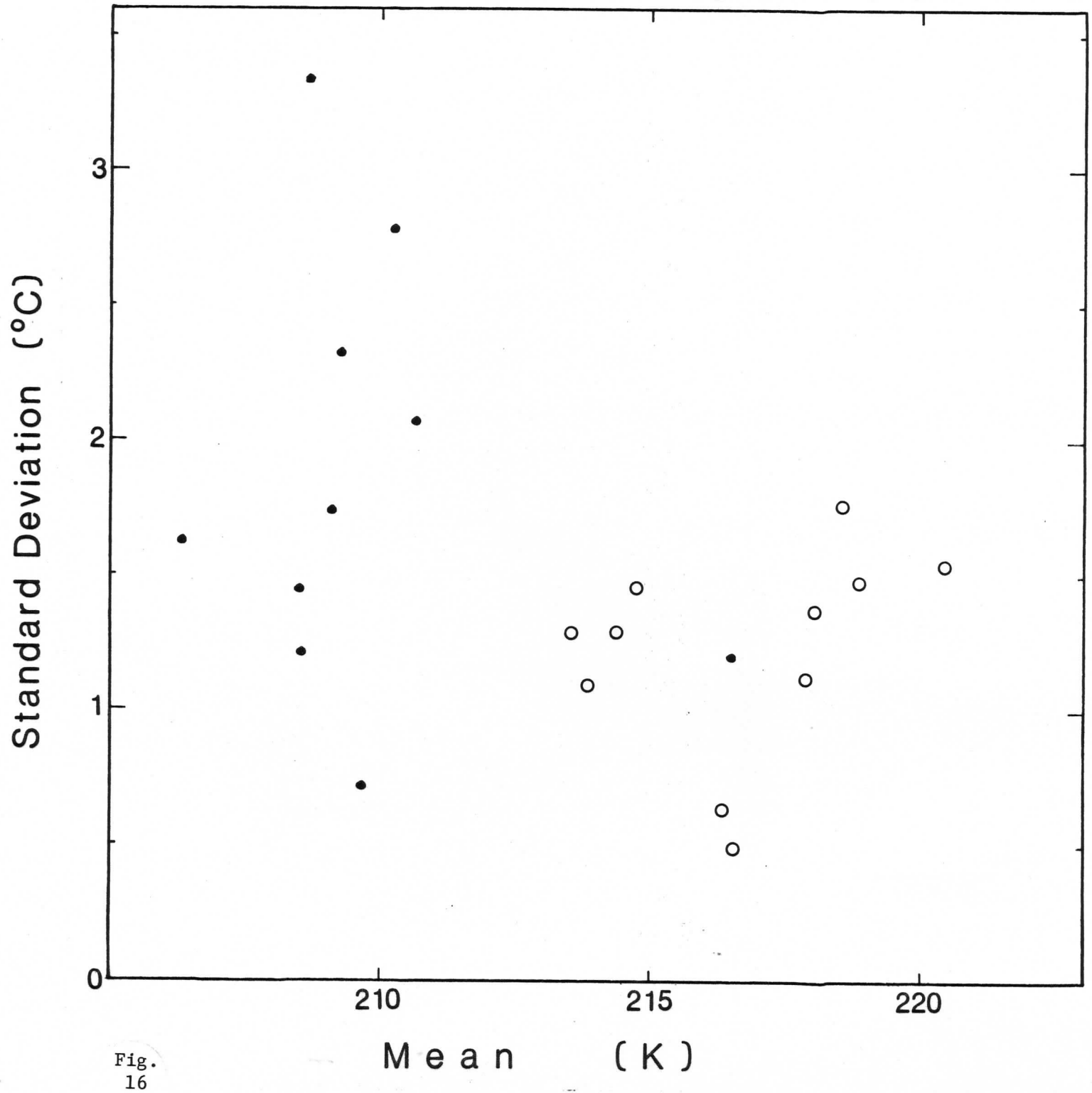

Fig.
16

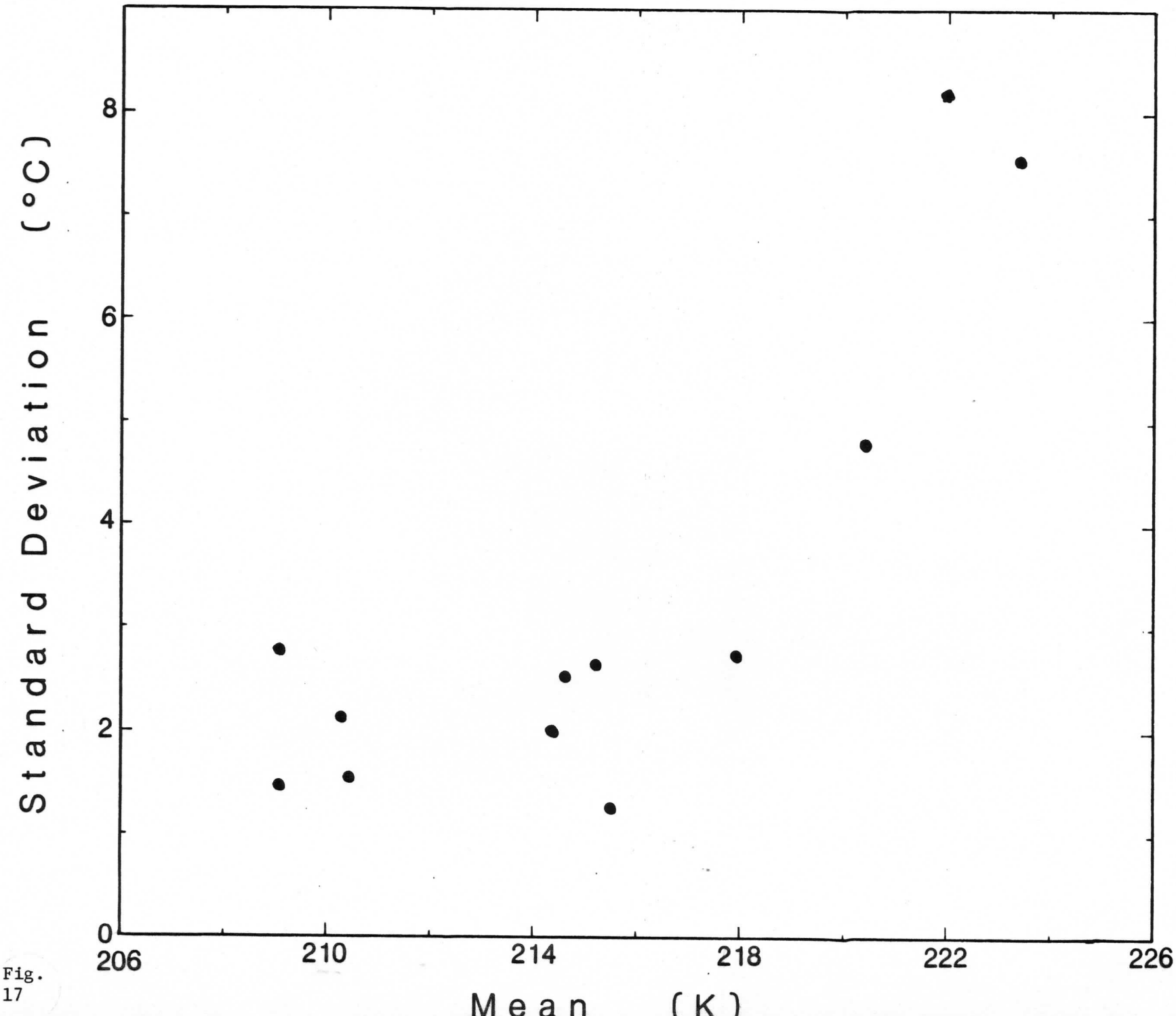

Fig. 17

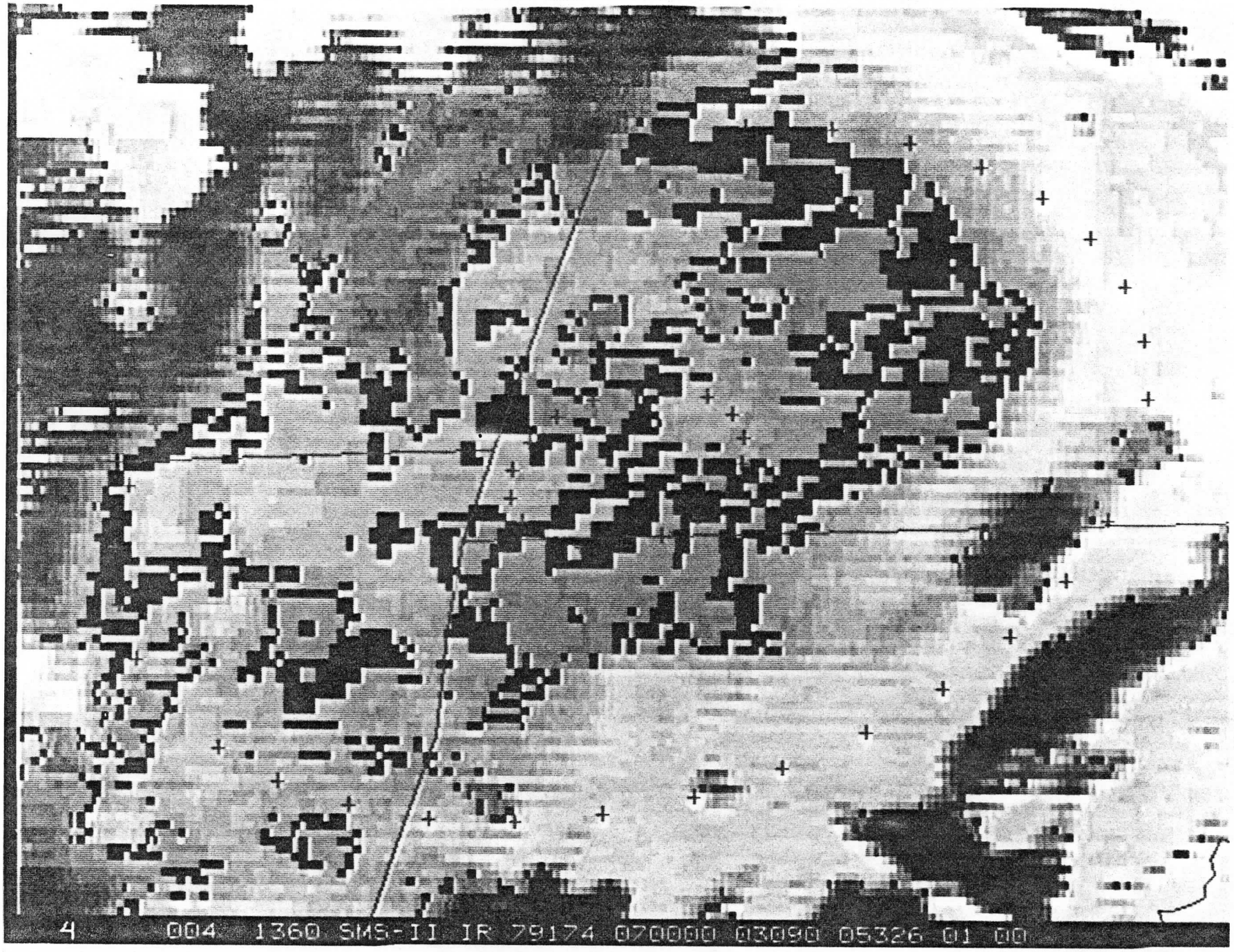

Fig.
18

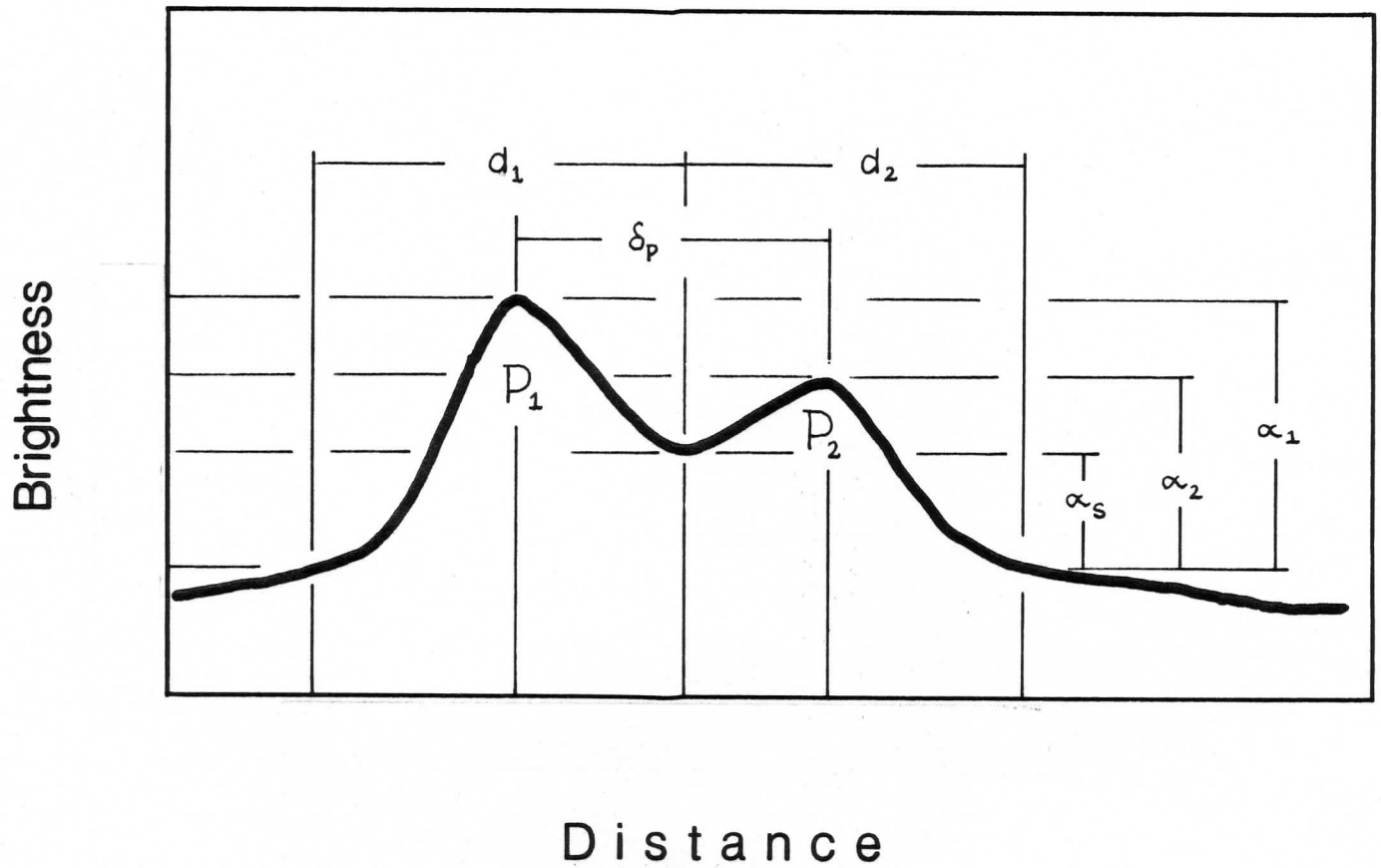
Brightness
d_1
d_2
δ_p
P_1
P_2
α_1
α_2
α_s
Distance

Fig. 19